INFORMATICS JOURNALS
The Journal of Electrochemical Society of India, Volume 74, Issue (3&4), April – June 2025; pp. 79–96
ISSN (Print) : 0013-466X
ISSN (Online) : xxxx-xxxx
DOI: 10.18311/JESCI/2025/51687

An Overview of Corrosion Performance of Zr and Ni-based Metallic Glass Alloys and Coatings for Highly Corrosive Environments

Chiranjit Poddar[1,2], S. Ningshen[1,2*]and U. Kamachi Mudali[2]

[1]Corrosion Science and Technology Division, Metallurgy and Materials Group, Indira Gandhi Centre for Atomic Research, Kalpakkam-603102, India

[2]Homi Bhabha National Institute, Anushaktinagar, Mumbai 400094, India

Abstract:

In recent decades, Metallic Glass Coatings (MGCs) have attracted great interest due to their practical applications and scientific importance in several industries. The present paper provides an overview of developing corrosion-resistant Zr and Ni-based MGCs for aggressive environment applications like in sodium chloride, hydrochloric acid, and nitric acid media. The microstructure, thermal stability, surface morphology, and hardness of the Zr and Ni-based MGCs are briefly discussed. The corrosion resistance of MGCs is highlighted based on surface roughness, coating thickness, composition, and the nature of the passive film properties. Furthermore, the corrosion resistance of Zr and Ni-based amorphous metallic coatings as a suitable engineering material for industrial applications in aggressive environments are provided. The current challenges towards the practical applications and development of highly corrosion-resistant MGCs and their requirements for future development are also highlighted, with a few emphases on using magnetron sputtering coating.

Keywords: Acid Solution, Magnetron Sputtering, Metallic Glass Coatings, Passive Film, Polarisation, XPS

1. Introduction

Bulk Metallic Glasses (BMGs) are an emerging family of superior engineering materials associated with desirable and highly attractive properties, ranging from excellent hardness, oxidation resistance, outstanding corrosion resistance, and good mechanical strength[1-8]. In the last two decades, enormous papers were published related to the synthesis and properties of BMGs, mainly in the form of cast, laser processing, thermal, and cold spray etc.[9-11] Axinte *et al.* discussed the history of BMGs, their unique properties, and their applications.[12] A detailed review of the BMGs, considering casting, thermoplastic forming, and their effect on the material properties, has been discussed in detail by Schroers *et al.*[13] The suitability of glass formation of BMGs, considering the role of minor alloying addition and their effect on the material properties, has also been reviewed[14,15]. Scully and Gebert[16] also reported superior corrosion resistance and good mechanical properties of the various Zr-based cast BMGs.

The corrosion behaviour of the numerous bulk metallic glass systems, for example, Fe, Ni, Zr, Al-based, Cr, Cu, Mg, and Ti-based systems, was studied in various corrosive environments[1,16,17-20]. Arc-melted Ni and Zr-based BMGs indicated good corrosion resistance with their ability to form a stable and protective passive film[21-24]. The Zr-based alloy of composition $Zr_{54}Ni_{44}$, $Zr_{64}Cu_{16}Ni_{10}Al_{10}$, $Zr_{58}Cu_{16}Ni_{13}Al_{10}Nb_3$, and $Zr_{46}Cu_{37.6}$ $Ag_{8.4}Al_8$ metallic glasses exhibited higher corrosion resistance in an aggressive environment, attributed to the protective ZrO_2 passive film.[21,23,25] Moreover, the Ni-based BMGs rods and ribbons (micro-alloying with refractive elements Nb, Ta, Zr, and Ti) of composition $Ni_{60}Nb_{40}$, $Ni_{60}Nb_{30}Ta_{10}$, $Ni_{45}Nb_{25}Zr_{25}$, Ni-Nb-Zr-Ti, Ni-Nb-Zr-Ti-Ta, etc.[18, 26-28] The Zr and Ni-based BMG are highly corrosion resistant attributed due to their protective, stable, and self-adherent

*Email: ning@igcar.gov.in

passive film. They also exhibited good wear resistance; however, the rapid shear bands spread during plastic deformation, and lower ductility at temperatures below the glass transition limited the applications[29]. In addition, real-time applications and commercialisation of BMGs are challenging because of the difficulty in fabricating more than 10 mm-thick sheets or manufacturing into a complicated shape. The critical cooling rate for freezing molten liquid without inducing crystallization is inversely proportional to the square of the thickness ($1/t^2$) and directly proportional to the thermal diffusivity (κ) of the sample (κ): T_{cr} $/t^2$. A critical cooling rate required to achieve an amorphous structure in a thick sheet, difficult in present technologies[30]. So, obtaining a homogeneous MG's κ along with the uniform thickness is crucial for the BMG material.

MGCs can circumvent the disadvantages of BMGs' corrosion attack and increase the applicability of BMGs for many other potential applications. Further, the physical and chemical properties can be tailored, and the mechanical properties can be enhanced by changing their chemical composition[31,32]. The ductility and yield strength of metallic coatings, ceramic coatings, and thin film metallic glasses are superior to those of bulk metallic glass[33]. Recently, research has been performed on the use of thin-film metallic glasses for MEMS applications[34]. Studies also showed that thin-film metallic glasses, which exhibited similar features to traditional hard-coating materials, are similar to BMGs used in thin film form[35].

In the last decades, several BMGs in the form of coatings on engineering materials have been developed in the range of 100 microns to nanometer thickness[31,36]. Different high-energy techniques are used to synthesize metallic glass coatings, including high-velocity oxygen fuel spray, vacuum plasma spray, pulsed laser deposition, etc.[25,36,37]. In addition, the production of metallic glass by sputtering costs much lower than cast BMGs[38]. The cost can be reduced in two ways: Firstly, the cooling is avoided using gaseous condensation, so the material system can be replaced by cheaper elements[36]. Secondly, as the sputtering parameters are adjustable, the materials can be designed for different metallic glasses[39].

2. Fabrication of the Metallic Glass Coatings: Magnetron Sputtering

Physical vapour deposition, including the sputtering technique and laser deposition, is the most suitable process to produce a metallic glassy coating with an amorphous structure because the process can randomly deposit the atomic layer[31]. It also provides a high cooling rate, which is necessary to quench the sputtered atoms into a glassy state. During the coating development, a wide range of temperatures is applied to the substrate to obtain optimized mechanical performance of the coating[40]. In order to retain an amorphous structure of the coating during deposition, the substrate operating temperature could range from room temperature to 200°C or higher, although this again depended on the glass-forming ability and alloy composition. The significant advantages of the sputtering technique in developing corrosion barrier coatings are the amorphous nature obtained on a larger surface area, easy fabrication in a short time, direct coating on the engineering structural material, etc.[41] Moreover, the sputtering technique is considered a non-equilibrium process; hence, it is beneficial to obtain an amorphous structure[33]. The reported BMG coating processing techniques and parameters, such as thickness and surface roughness, are shown in Table 1.

New MGC coatings have been developed in recent years with fascinating and improved performance, such as corrosion resistance, mechanical properties, and biocompatibility, by altering their alloying element compositions.[4,32] Thicker or thinner film metallic glasses, ranging from 3 to 6 μm, are produced using Zr-TL (late transition metal TL = Cu, Co, Ni) on Si substrate via the magnetron DC sputtering method with different deposition parameters[42,43]. The composition of BMGs traditionally follows Inoue's three empirical rules to achieve a glassy structure in the amorphous matrix, wherein the atomic size mismatch among alloying elements should be more than 12%[44]. For example, Deng *et al.,* fabricated a novel Zr-Ti-B-Si BMG coating by co-sputtering individual elements, and this system exhibited good hardness and corrosion resistance[45]. Similarly, the binary of atomic pairs shows a negative heat of mixing with the exception of the Zr-Ti couple, and the atomic size mismatch between Zr and B atoms is 82.8%. One prominent Zr-based MGC, Zr-Cu-Al-Ni metallic glass coating with an amorphous structure, was produced by sputtering techniques[38]. However, the sputter addition of Si in $Zr_{61}Al_{7.5}Ni_{10}Cu_{17.5}Si_4$ metallic glass coating reveals a typical homogeneous amorphous matrix with a dispersed nano-crystalline phase[33].

Few Ni-based coatings of composition $Ni_{50}Nb_{50}$, $Ni_{60}Nb_{40}$, and multi-layered $Ni_{50}Nb_{50}/Ni_{60}Nb_{40}$ (at.%)

Table 1. Reported BMG coating processing techniques and parameters, such as thickness and surface roughness

Metallic glass	Process	Thickness (nm)	Roughness (RMS in nm)	Reference
$Zr_{50}Cu_{50}$	Magnetron Sputtering	4100	2.34	31
$Zr_{38}Cu_{62}$	Magnetron Sputtering	3200	4.25	31
$Zr_{57}Co_{43}$	Magnetron Sputtering	3100	30	42
$Zr_{54}Ni_{46}$	Magnetron Sputtering	3200	29	42
$Zr_{46}Ti_{56}$	Magnetron Sputtering	300	-	48
$Zr_{65}Cu_{15}Al_{10}Ni_{10}$	Magnetron Sputtering	100-1000	0.7-1	6
$Zr_{53}Cu_{33}Al_{9}Ta_{5}$	Magnetron Sputtering	100	1.06	50
$Zr_{48}Cu_{36}Al_{8}Ag_{8}$	Magnetron Sputtering	1500-2000	0.45	30
$Zr_{59}Ti_{3}Cu_{20}Al_{10}Ni_{8}$	Pulse Laser Deposition	250	1	25
$Ni_{50}Nb_{50}$	Magnetron Sputtering	1000	1.86	46
$Ni_{60}Nb_{40}$	Magnetron Sputtering	1000	1.96	46
$Ni_{60}Nb_{30}Ta_{10}$	Magnetron Sputtering	2000	2	9
$Ni_{60}Nb_{30}Zr_{10}$	Magnetron Sputtering	2000	2.3	9

MGCs were also fabricated using magnetron sputtering, and such MGCs appear promising with high corrosion resistance coating due to their micro-structural and physicochemical advantages[46]. Recently, we successfully deposited 2 µm thick $Ni_{60}Nb_{30}Ta_{10}$ and $Ni_{60}Nb_{30}Zr_{10}$ metallic glass coatings on type 304 L SS substrate at room temperature.

3. Microstructure of Zr and Ni-based MGCs

A comprehensive microstructure analysis is required to develop potential corrosion applications of MGCs. The microstructure of MGCs has great importance for corrosion processes, as it usually determines the passive film stability of the alloys[46].

The XRD patterns of various Zr-based MGCs with different compositions exhibited an apparent broad hump (Fig. 1a), indicating the formation of an amorphous structure. Zeman *et al.* reported co-sputtered $Zr_{100-X}Cu_{X}$ (X ranges from 18 at.% % to 88 at.% %) MGCs at low charge density exhibited a fully amorphous structure[47]. The tendency to form a metallic glass structure in a wide range of compositional proportions against crystallization has been reported[32]. Chen *et al.* reported the effect of vacuum annealing at different temperatures of co-sputtered $Zr_{45}Cu_{55}$ and Zr_{54}-Ti_{46} metallic glass coating deposited on the Si substrate[48]. After one hour of isothermal annealing at 300°C, $Zr_{45}Cu_{55}$ films do not undergo any crystallization peak. However, a few crystalline peaks appeared as diffuse hump in the XRD pattern (Fig. 1b) after one hour isothermal annealing at 350°C, suggesting that the Zr_2Cu and Zr_7Cu_{10} nano-crystalline phases are embedded in the amorphous matrix. He *et al.* captured very short-range crystalline phases in the amorphous matrix by HRTEM image (Fig. 2a), and Cu nano-crystalline phases are confirmed by SAED pattern in as-deposited $Zr_{75}Cu_{25}$ metallic glass coatings[49].

The other binary couple of Zr-TL (TL= Ti, Ni, Co) MGCs with a significantly thicker coating have been fabricated using magnetron sputtering, varying the DC power[43]. Moreover, nano-crystalline Zr-Ti phase particles at high sputtering power are reported on the HREM lattice cross-sectional view in $Zr_{54}Ti_{46}$ MGCs (Fig. 2b).

The Zr-Ni and Zr-Co metallic glass thin films with extensive glass-forming range exhibited broad, amorphous hump using the co-sputtering, indicating such systems have a more remarkable Glass-Forming Ability (GFA)[42]. Their crystallization behavior upon the heat treatment is shown in Fig. 1(b). The Zr-Co is relatively more thermodynamically stable compared to the Zr-Ni coating. Also, the Zr-Co coating forms ortho and meta ZrO_2 along with ZrCo intermetallic phase at 440°C. The quaternary and ternary Zr-Cu-Al-Ni (Fig. 1a), Zr-Cu-Ni-Ta, Zr-Cu-Ni, and MGCs

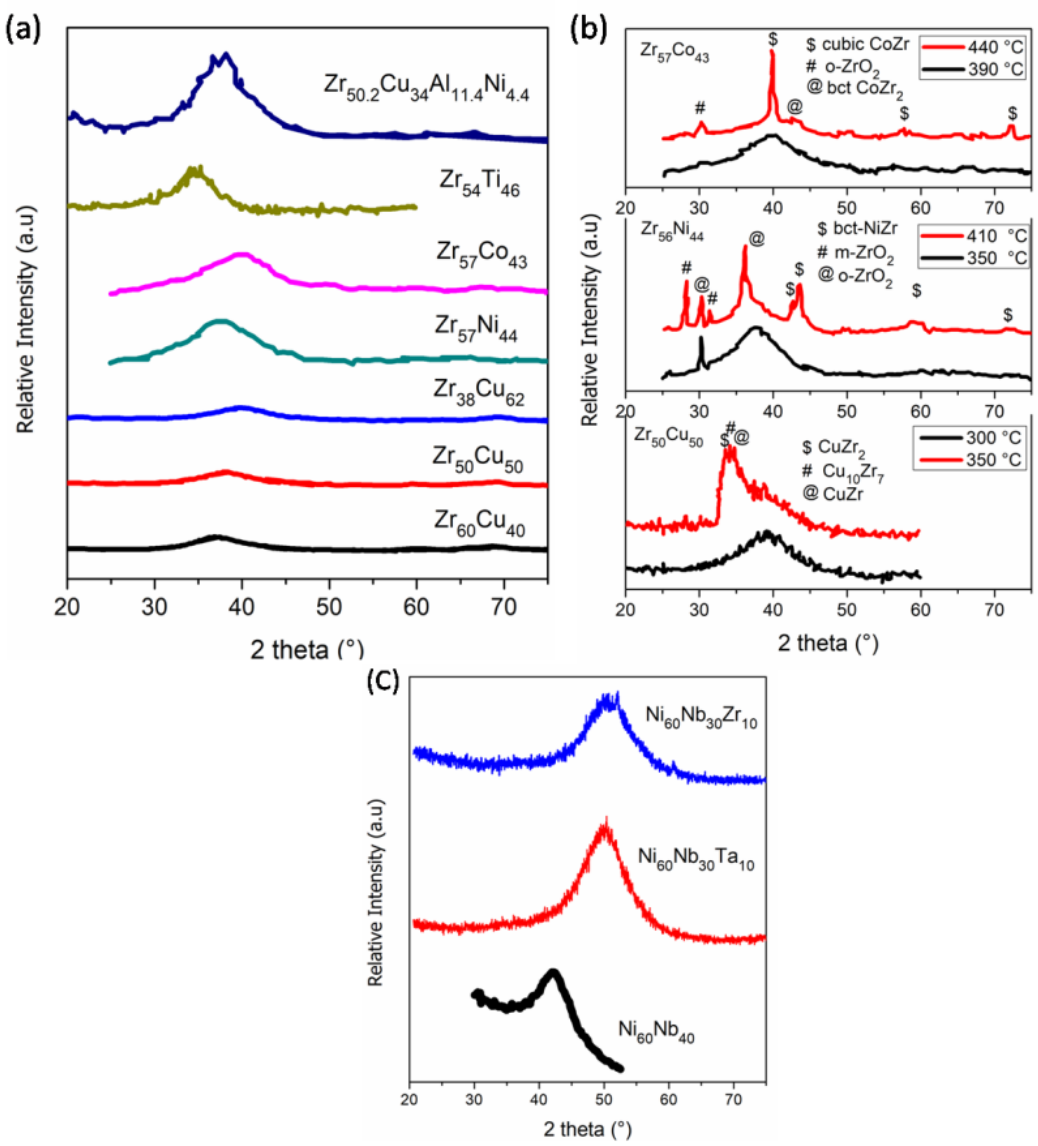


Figure 1. XRD patterns of **(a)** various thick Zr-based metallic glass coatings deposited on either Si or stainless-steel substrates using magnetron sputtering and **(b)** the binary Zr-Co, Zr-Ni, and Zr-Cu system under elevated temperature annealing condition[42], **(c)** the Ni-based metallic glass coatings of composition Ni_{60}-Nb_{40}, $Ni_{60}Nb_{30}Ta_{10,}$ and $Ni_{60}Nb_{30}Zr_{10}$ metallic glass coatings[9].

with extraordinary GFA are prepared by magnetron sputtering coatings, with a fully amorphous structure[50,51]. Lee *et al.* added nitrogen to produce Zr-Cu-Ni-Al-N MGCs via a DC magnetron sputtering on p-type (100) silicon wafers substrate[52], and it also exhibited an amorphous structure. However, Chuang *et al.* fabricated coatings with a different nitrogen flow rate on the Zr-Ni-Al-Si system and observed that Zr-Ni-Al-Si-N0 exhibits only an amorphous structure[53]. HRTEM images of ternary Zr-Cu-Ni-Al and Zr-Cu-Ni-Ta coating with no short-range crystalline ordering, indicating the complete metallic glassy structure (Fig.2c-d)[51,52].

The XRD diffraction pattern in Fig. 1c also indicates the feasibility of forming the Ni-based metallic glass coatings considering the Nb, Ta, and Zr refractory alloying elements.

4. Thermal Stability of Zr-based Metallic Glass Coatings

The Zr-based Zr-Cu MGCs show a remarkable GFA, resulting in extensive thermal stability in various compositions (Table 2)[47]. One of the main reasons for the greater thermal stability of the Zr-Cu alloy system

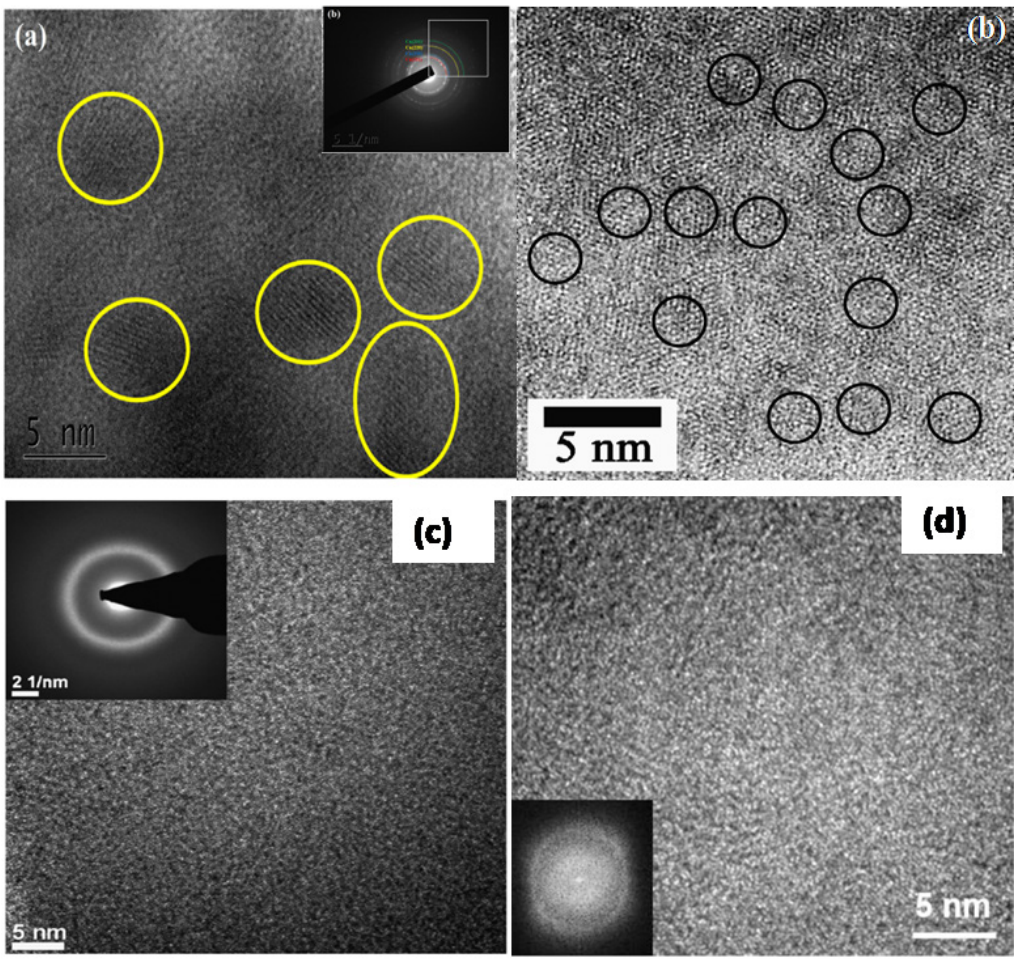


Figure 2. HRTEM image **(a)** nano-crystalline particles of as-deposited $Zr_{75}Cu_{25}$ coatings in the circle marks[49] and **(b)** lattice cross-sectional-view of the $Zr_{54}Ti_{46}$ thin film produced high sputtering power[48] **(c)** Zr-Cu-Ni-Al, and (d) Zr-Cu-Al-Ta metallic glass coatings[50].

Table 2. Glass transition temperature T_g (°C), crystallization temperature T_c (°C), and super-cooled liquid region $\Delta T = T_g - T_c$ of the Zr-Cu films deposited at the low density (LD) 0 and high density (HD) discharge current-voltage conditions[47].

LD Condition								
Zr (at. %)	69	64	60	54	49	45	-	38
T_g	357	373	385	400	417	426	-	463
T_C	399	416	429	447	464	475	-	507
ΔT	42	43	44	47	47	49	-	44
HD Condition								
Zr (at. %)	70	-	58	53	51	47	40	35
T_g	348	-	382	406	411	424	447	466
T_C	376	-	415	445	453	468	482	500
ΔT	28	-	33	39	42	44	35	34

is APD (Atomic Packing Density), i.e., the native arrangement of atoms. The APD correlated structure and properties of Zr-Cu metallic glass were explained in detail by Park *et al*[54]. The quaternary Zr-Ni-Al-Si MGCs were fabricated by Chuang *et al.*, and elucidated DSC results of the coatings with different nitrogen flow rates or percentages of target poisoning[53]. The Zr-Ni-Al-Si-N0 and Zr-Ni-Al-Si-N1 exhibited T_g and T_x, while other nitrogen-containing Zr-Ni-Al-Si do not show T_g and T_x. Rajan *et al.* reported a T_{rg} of 0.3473 for Zr-Cu-Ag-Al MGCs, and it is also a significant indicator of the alloy to form a metallic glassy structure[30]. The Zr-Cu-Ni-Al-N show good T_g, $T_{x,}$ and ΔT at 525, 615, and 90 °C, respectively, which indicates high thermal stability[52]. The MGC exhibited an amorphous structure up to the T_g and exhibited superior plastic properties within ΔT. However, it was found to crystallise completely after the annealing

temperature reached 740°C. Chuang, et.al., investigated the effect of the fluorine and sulfur addition in specific ratios on the thermal stability of Zr-Ti-Ni MGCs, known as SF6_0, SF6_0.1, SF6_0.2, SF6_0.3, and SF6_0.4[55].

5. Metallic Glass Coating - Surface Morphologies

The surface morphology of sputter-deposited $Zr_{50}Cu_{50}$ and $Zr_{38}Cu_{62}$ MGCs films shows vertically aligned columns, a typical micro-structure of a physically grown film by magnetron sputtering.[32] The microstructure was achieved by adjusting the incident angle and rotating the substrate at a constant speed[56]. The surface morphologies of Zr-Cu with globules clusters with voids and micro-crack are evident. The top surface shows a typical nano-glassy microstructure of complex hierarchy-type shapes. The nano-clusters are regarded as building blocks, agglomerated into a larger globule size of 50-70 nm. Such nanostructures were also observed in other Zr-based MGCs obtained by magnetron sputtering. The isotropic growth of glassy clusters results to cracks and pores on the surface of the coating[57]. This provide atomic density variation and free volume in the amorphous structure for Cu-Zr films. This morphology is typically referred to as a cauliflower-like structure[32]. In addition, smaller nano-columns and smoother nano-granular structures can also be achieved by tuning the sputtering parameters for better performance (Fig. 3)[32]. Other binary, sputtering processes, ternary, and quaternary Zr-based metallic glass coatings also exhibited similar surface structures, with varying sizes of the column width and globules of spheroid clusters structure[41].

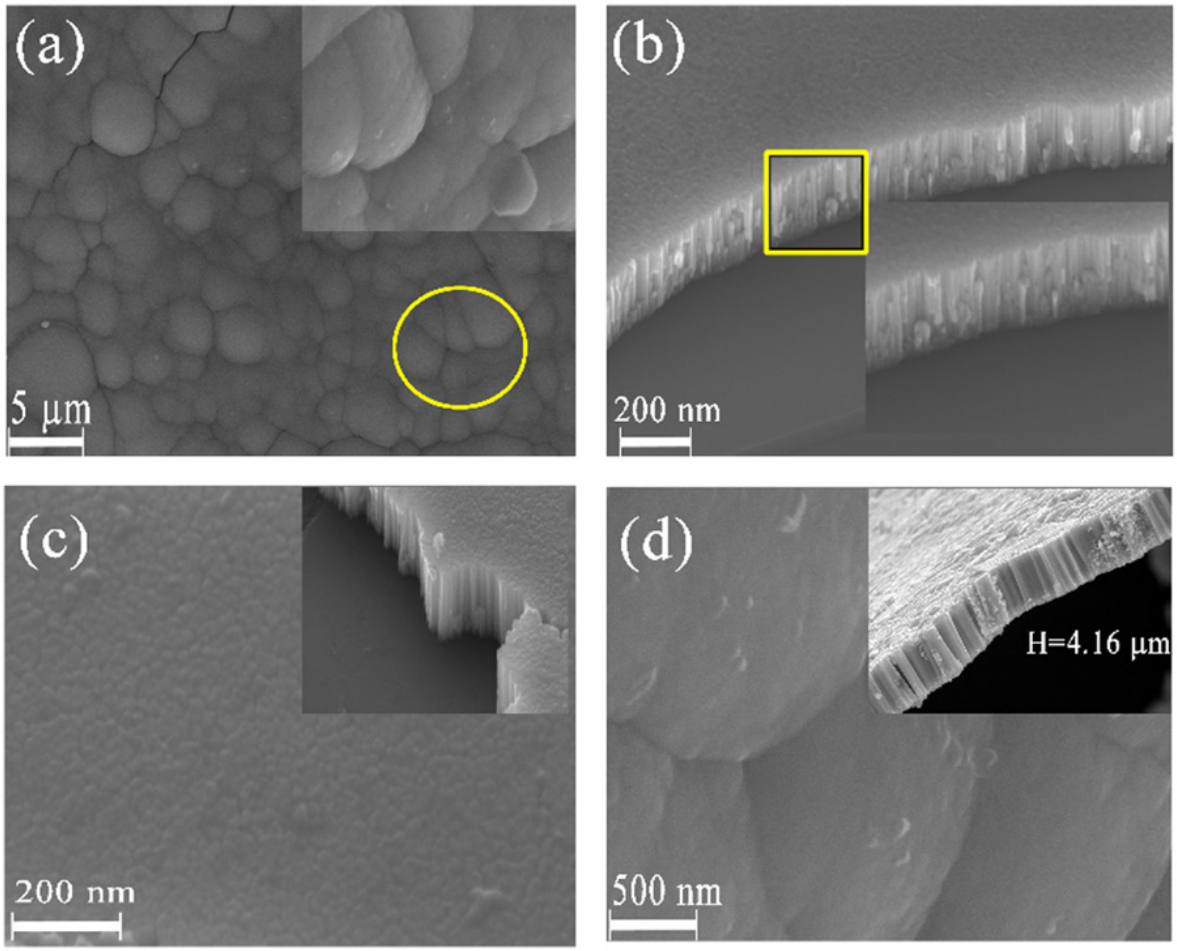


Figure 3. FESEM of $Cu_{50}Zr_{50}$ metallic glass coating with a typically nanogranular structure. **(a)** Film surface with enlarged images, **(b–d)** Cross-section and high-resolution SEM of the showing granular morphology - (yellow circle and square represent the grain boundaries and typical morphology zone)[32].

In addition, the corrosion properties depend on the roughness of the coating surface and sometimes also its thickness. The RMS roughness values of Zr-based MGCs coatings for their different thickness and presented in Table 1. The AFM surface measurements of the thin film revealed that sputtering conditions influence the film surface roughness[32]. The smooth surface and nano-glassy structure 2D AFM images (Fig. 4(a-b)) of $Cu_{64}Zr_{36}$ and $Zr_{50}Cu_{50}$ MGCs[32]. The typical surface topography of $Zr_{59}Ti_3Cu_{20}Al_{10}Ni_8$ MG coated on type 304L SS of different thicknesses using AFM are shown in Fig. 4(c) and (d), respectively[6].

Jiang *et al.* developed mono-layered $Ni_{50}Nb_{50}$, $Ni_{60}Nb_{40}$, and the multi-layered $Ni_{50}Nb_{50}/Ni_{60}Nb_{40}$ MGCs by using DC magnetron sputtering[46]. The SEM morphologies of the Ni-based MGCs with their corresponding AFM 3D images are shown in Fig. 5 (a,b,c). The surface of the MGCs shows globular shape morphologies. But the globule size is smaller in $Ni_{60}Nb_{40}$ MGC compared to the $Ni_{60}Nb_{30}Ta_{10}$ and $Ni_{60}Nb_{30}Zr_{10}$ MGCs attributed to agglomeration of the small irregularities during the growth on the type 304 L SS substrate. The EDS mappings of MGCs showed the uniformly distributed Ni and Nb elements on the Ni-Nb coating surfaces[46]. The resultant homogeneous surface morphology by magnetron sputtered coatings block the corrosive species diffusion in corrosive environment. On the other hand, the cross-sectional images indicated that the columnar structure and column are very much diffused from each other (Fig. 5 (d-e)). The surface roughness of the Ni-based MGCs samples was measured by AFM and presented in Table 2. The RMS roughness is relatively smaller (nano-scale roughness), and insignificant differences amongst the Ni-based MGCs have been noticed in roughness values. The AFM morphologies indicated relatively homogeneous deposition of different Ni-based MGCs, suitable and desirable for high corrosion resistance[46].

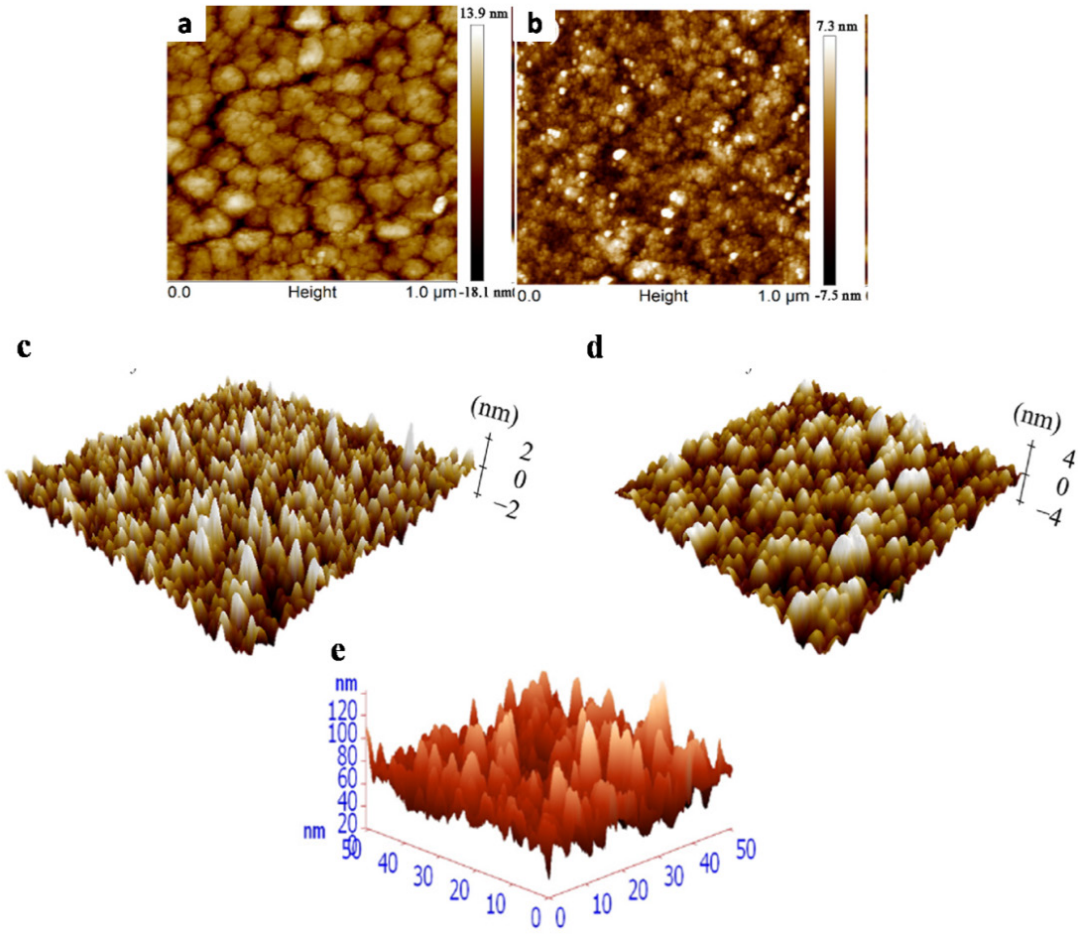


Figure 4. AFM topographies of **(a)** 2D $Cu_{64}Zr_{36}$ [61] **(b)** 2D $Cu_{50}Zr_{50}$ [61] **(C)** 3D $Zr_{59}Ti_3Cu_{20}Al_{10}Ni_8$ with 100 nm thick[6] **(d)** 3D $Zr_{59}Ti_3Cu_{20}Al_{10}Ni_8$ with 1000 nm thick[6], and **(e)** 3D $Zr_{59}Ti_3Cu_{20}Al_{10}Ni_8$ metallic glass coatings samples[25].

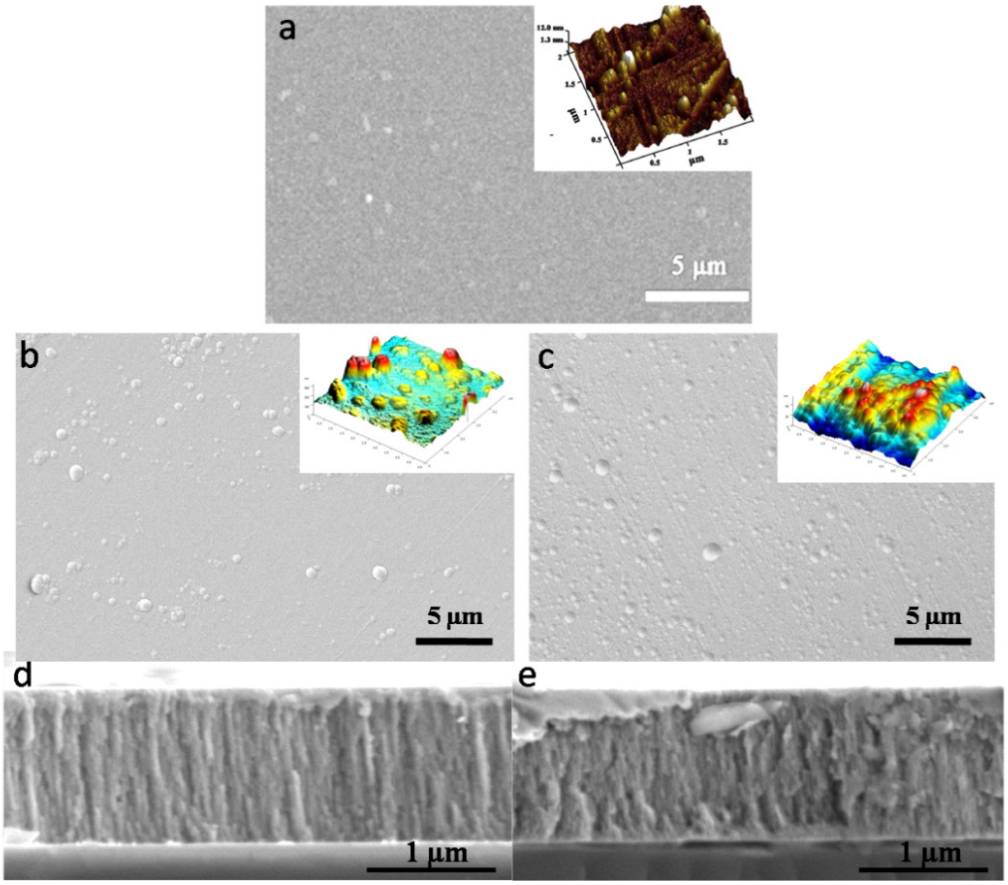


Figure 5. Surface morphology and their corresponding AFM images of **(a)** $Ni_{60}Nb_{40}$[65], **(b)** $Ni_{60}Nb_{30}Ta_{10}$ **(c)** $Ni_{60}Nb_{30}Zr_{10}$ metallic glass coating deposited on stainless steel; Cross-sectional images of **(d)** $Ni_{60}Nb_{30}Ta_{10}$ **(e)** $Ni_{60}Nb_{30}Zr_{10}$ metallic glass coating[9].

6. Corrosion Behavior of Metallic Glass Coatings

6.1 Corrosion Behavior of Zr-based Metallic Glass Coatings

Currently, Zr-based MGCs are the most investigated coatings among the other MGCs or as thin films. The corrosion property of Zr-based MGCs was studied in different corrosive environments, such as 3.5 wt% aqueous NaCl solution[49], 1 M HCl[51], 11.5 M HNO_3[25], and other solutions[31].It has been reported that the Zr-coated specimens exhibited higher E_{corr}, lower I_{corr}, and lower I_{pass} when compared to crystalline materials like Ti alloys and stainless steel[31]. From a structural point of view, the good corrosion resistance of the coatings also depends on the (i) solid solution phase comprising chemical uniformity, good structure without any micro-structural defects, and (ii) the ability to form single solid solutions by additions of an alloying element such as beneficial refractory metals, transition metals, and rare-earth elements. The multi-component Zr-based bulk metallic glass exhibited excellent corrosion resistance in a halide-free environment over a large pH range at room temperature[25,42]. Apreutesei et al carried out the potentiodynamic polarization test of Zr–Ni and Zr–Co amorphous films and their crystallization counterpart in the aerated Na_2SO_4 solution (Fig. 6)[42]. The cathodic part in Tafel's plot suggests the same reactivity occurring at the surface of both MGCs, which further implies a charge transfer control of the reduction process. Microalloying elements like Ni and Co do not significantly affect the E_{corr} value, nor the corrosion current densities, and the typical passive current densities of 1–10 µA/cm^2 for both coatings. On the other hand, the corrosion properties of Co-containing as-deposited film and its annealed crystalline counterpart are almost unchanged: Crystallization effects on corrosion have already been reported for other Zr-based BMGs[31,58,59].

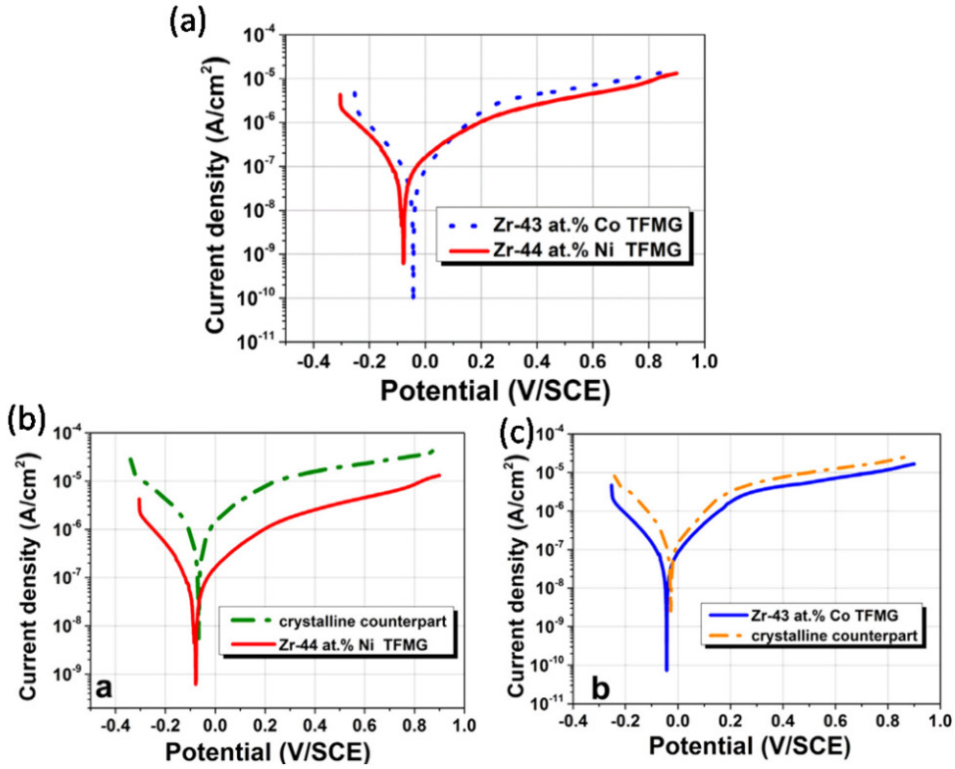


Figure 6. Potentiodynamic polarization curves in $NaSO_4$ solution for **(a)** as deposited amorphous Zr-Co and Zr-Ni MGCs, **(b)** Zr-Ni MGC and its crystalline counterpart as well as **(c)** Zr-Co MGC and its crystalline counterpart.[42]

The potentiodynamic polarization curves for as-deposited annealed $Zr_{75}Cu_{25}$ MGCs and bare 304 SS substrate in 3.5 wt% NaCl solution are shown in Fig. 7(a)[49]. Under annealing conditions at 350°C, ZrO_2 oxide nanoparticles is formed on the surface, shifting the E_{corr} value towards a nobler direction than the as-deposited MGCs. The i_{corr} values for as-deposited and annealed MGCs in 3.5 wt% NaCl were notably lower than bare 304 SS substrate, which confirms the improved corrosion resistance of the 304 SS after ZrCu coatings. Furthermore, the as-deposited sample shows the least i_{corr} value, which indicates better performance in terms of corrosion resistance. After polarization studies, the 304 SS substrate showed a typical undercutting in discontinuous circular form and lacy morphology (Fig. 7 (b-e)), of pitting corrosion[49]. The scurfs appearance was detected on the surface of $Zr_{75}Cu_{25}$ coatings, in which the copper coatings were relatively low (less than 5%). This implies that the Cu probably negatively affected the corrosion resistance. The insightful observation shown by Tang et al. indicated the increase zirconium and oxygen variations, while Cu remained marginal at a distance from the boundary[60] Jang *et al.* reported the effect of vanadium (V) addition Zr-Cu-Al-Ni and Zr-Ti-Al-Ni magnetron sputtered coatings on the corrosion behavior[36]. The Zr-Ti-Al-Ni-V coatings exhibited partial nanocrystals embedded in the amorphous matrix structure, while the Zr-Cu-Al-Ni coating had a fully amorphous structure with very low surface roughness (1 nm). Both coatings performed well without any pitting corrosion.

Chuang *et al.* studied the corrosion behavior of quaternary Zr-Cu-Ni-Al MGCCs on Si and AISI 402 substrate in 1 M HCl aqueous solution[51]. The potentiodynamic anodic polarization parameters indicate that the Zr-based MGC shows good corrosion in HCl due amorphous and defect-free structure, compared to the bare AISI 402 stainless steel. Also, Cu-rich oxide corrosion products were reported for Zr-Ti-Cu-Al-Ni[61], and Mg-Cu-Ni-Ag-Zn-Gd-Y[62], BMGs. Kamachi Mudali *et al.*[61] studies also revealed a similar finding that suggested selective dissolution of Zr and Al elements. The ring-like corrosion patterns are formed mainly due to the extensive attack, as the reactive elements react with chloride ions (Fig. 8a)[51]. One of the particular types of corrosion path is a filiform

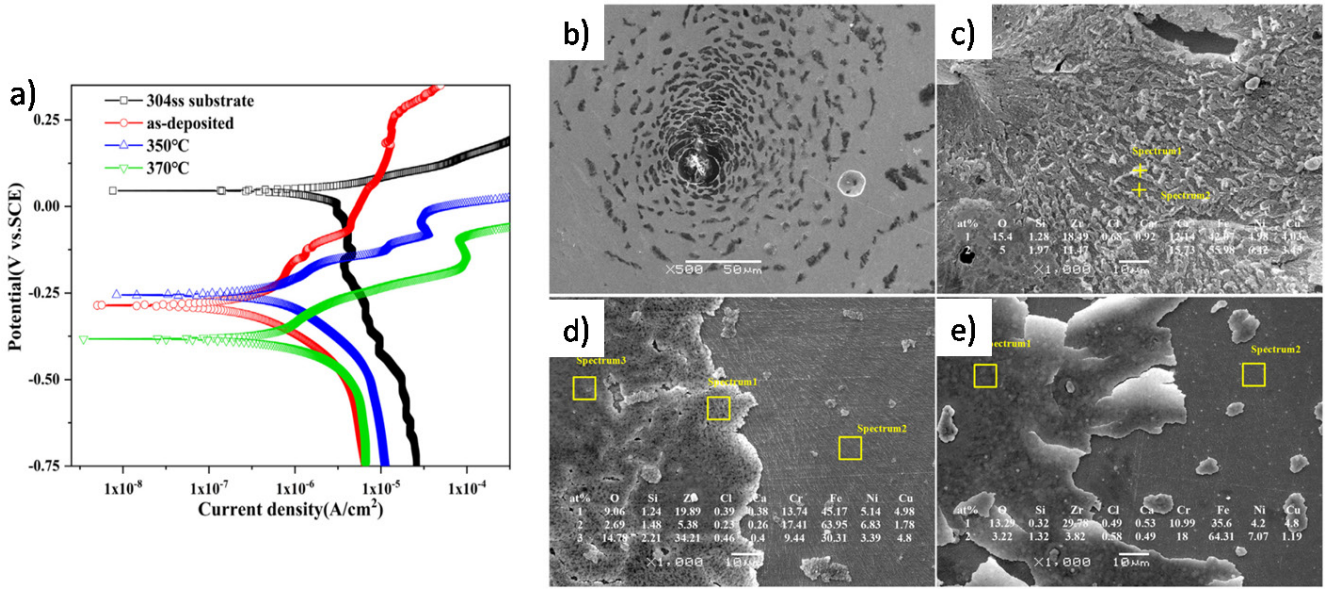


Figure 7. **(a)** Potentiodynamic polarization curves of as-deposited and annealed Zr-Cu metallic glass coatings and bare 304 ss substrate in 3.5 wt% NaCl solution; SEM and EDS images after polarization test of **(b)** bare 304 ss substrate **(c)** as-deposited Zr-Cu **(d)** oxygen annealed Zr-Cu at 350°C, and **(e)** annealed Zr-Cu at 370°C[49].

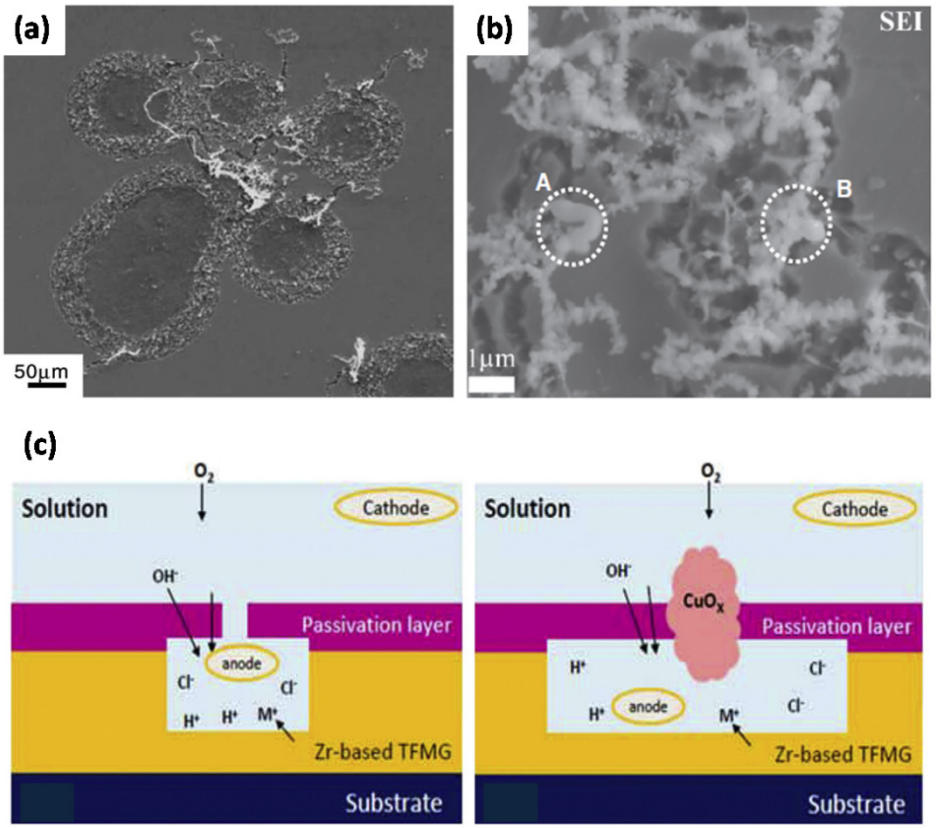


Figure 8. Corroded Zr-based metallic glass coating on AISI 420 substrate **(a)** secondary electron image of the filiform corrosion, **(b)** dashed circles of filiform corrosion A and B indicating the regions with higher contents of Zr, Cl, O and Zr, Al, Cl, O, respectively, and **(c)** the formation mechanisms of pitting corrosion and corrosion products on the pit[51].

type corrosion attack, as shown in Fig. 8b. The filiform-like corrosion developed when the filament propagated randomly from corrosion pits and surrounded the surface with passive layers. The mechanisms for the pitting corrosion reaction on the Zr-Cu-Ni-Al metallic glass coatings in the HCl environment have been discussed, and the schematic diagram is shown in Fig. 8c. Once a pit is initiated, it penetrates through the surface passive layer when the aggressive reactive element in the (Zr, Al) alloy is preferentially dissolved with chloride ions to form a river-flow pattern.

The anodic polarization of MG and MG-coated 304L SS in 1, 6, and 11.5 M nitric acid is depicted in (Fig. 9a). The corrosion current and passive current density increase with increasing nitric acid concentration, indicating the aggressiveness of concentrated nitric acid. Better corrosion resistance of pentanary Zr-based coated 304 L SS compared to bare 304 L SS in the nitric acid environment was evident. However, after the corrosion test, the surface roughness of the coating increased, which is attributed to corrosion-induced defects around secondary particles and thin MG-coated layer (Fig. 9b)[25].

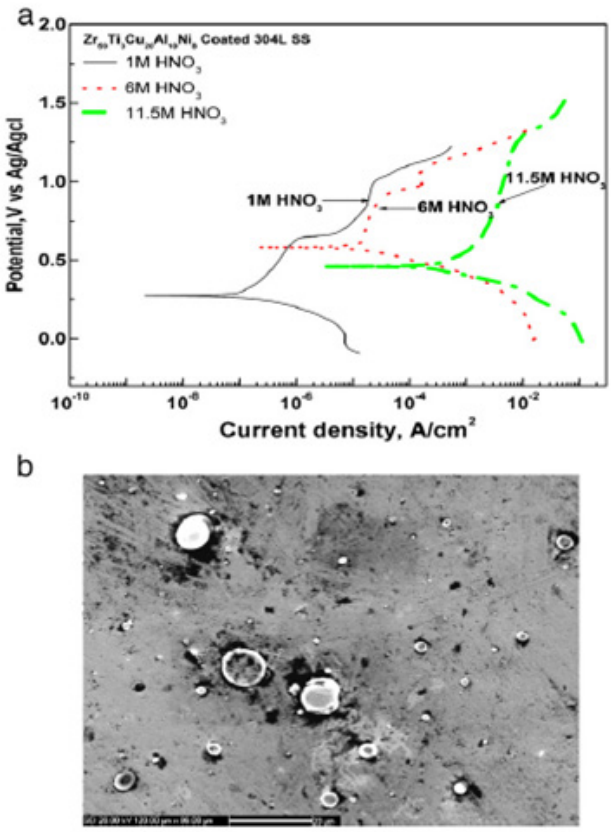


Figure 9. **(a)** Potentiodynamic anodic polarization plots of MG $Zr_{59}Ti_3Cu_{20}Al_{10}Ni_8$ alloy coated type 304L SS in 1 M, 6 M and 11.5 M HNO_3 and **(b)** SEM micrograph of $Zr_{59}Ti_3Cu_{20}Al_{10}Ni_8$ alloy coated type 304L SS after corrosion test in 11.5 M HNO_3 [Reproduced with permission from][25].

6.2 Ni-based Metallic Glass Coatings

The corrosion resistance of the magnetron sputtering processes of Ni-based MGCs is studied, and the inputs are compared to the Zr-based MGCs. Wu *et al.* studied the potentiodynamic anodic polarization tests of Ni-Nb MGCs with different thicknesses to investigate the changes in pitting susceptibility before and after coatings on type 316 L SS[62]. The potentiodynamic anodic polarization curves in 0.5 M NaCl solution for the uncoated 316L SS and Ni-Nb MGCs are shown in (Fig. 10a). The results reveal that the narrow and short passive region and the pitting corrosion are evident for the bare 316L SS specimen. On the other hand, relatively more stable and broader passive regions were observed for Ni-Nb MGCs at a passive current density of roughly 0.015 mA cm^{-2}. In addition, the pitting potential of the MG coatings increases with deposition time below 60 min, and remains unchanged after 60 min.

Further, the pitting corrosion morphological characteristics of the coating's specimens at different deposition times and bare type 316 L SS after anodic polarization tests in 0.5 M NaCl solution at a constant current density of 10 mA cm^{-2} are shown in Fig. 10 (b-e)[62]. During potentiodynamic anodic polarization tests, all the pits formed in a circular shape, and their depth, size, and density are presented in Table 3[33]. The pitting corrosion formed on the Ni-Nb coatings are smaller in size and higher in number than the bare 316 L SS, and this indicates that the pitting corrosion was negligible, and the pit nucleation is more dominant in the corrosion process. However, small fossettes-like features pits were observed in the Ni-Nb MGC coated on type 316L SS, but insignificant in the bare 316L SS. The probable reason for such fossettes is that pitting nuclei propagate more along the depth of the pits than the width.

The corrosion behavior of the sputter-deposited Ni-based MGCs on 304 L SS was compared with bare 304L SS. The potentiodynamic polarization tests on the $Ni_{60}Nb_{30}Ta_{10}$ and $Ni_{60}Nb_{30}Zr_{10}$ MGCs coated 304 L SS and bare 304 L SS were performed out in a high-concentration (11.5 M (Fig. 11a) nitric acid medium. The trans-passive region did not appear up to 1.6 V (Ag/AgCl)

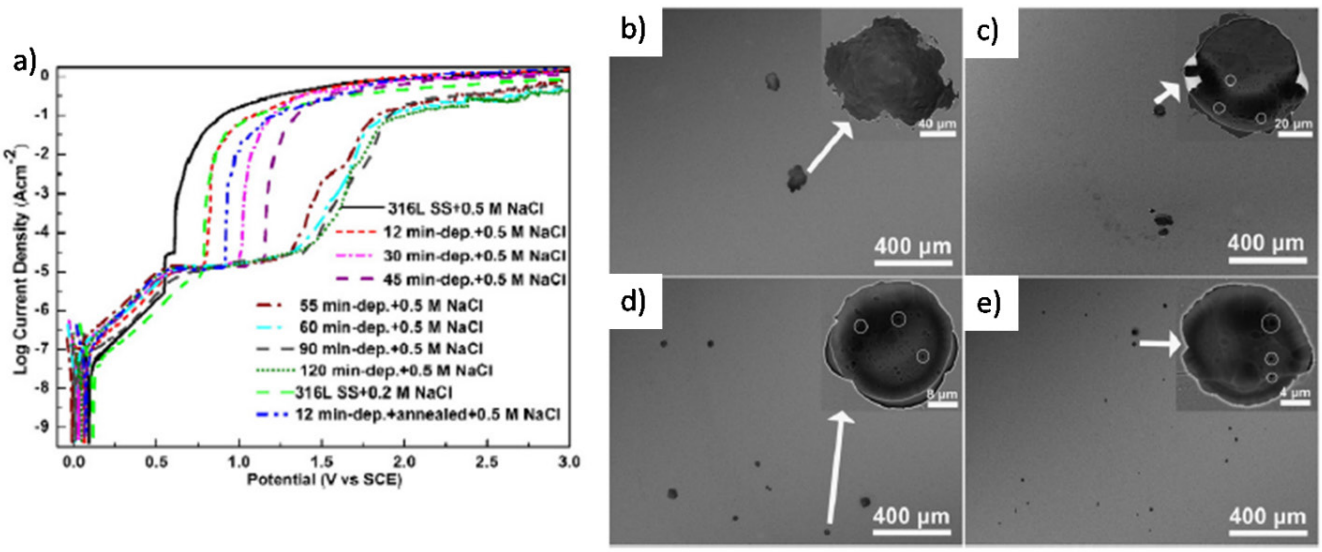


Figure 10. **(a)** Potentiodynamic polarization curves for bare 316 L SS and $Ni_{50}Nb_{50}$ metallic glass coatings on with different deposition time on 316 L SS substrate in NaCl solutions; Pits morphology after polarization on **(b)** bare 304 L SS **(c)** 12 min coating deposition **(d)** 30 min coating deposition, and **(e)** 60 min coating deposition[62].

Table 3. Statistics of the pits depth, size, and density on polarized bare 316 L SS and Ni-Nb metallic glass coating with different deposition time in 0.5 M NaCl solution at the current density of 10 mA/cm^2 [33].

Sample	316 L SS	TFMG-12 min	TFMG-30 min	TFMG-60 min
Depth (µm)	38.1	6.9	6.2	4.7
	30.3	5.2	4.3	2.6
Size (µm)	62.1	50.4	22.3	11.7
	52.3	30.2	17.9	8
Density (pits/mm^2)	0.8	1.6	3.3	8.6

for both the glassy coating[9]. In addition, the marginal differences in E_{corr} values between the $Ni_{60}Nb_{30}Ta_{10}$ and $Ni_{60}Nb_{30}Zr_{10}$ metallic glass coating samples indicate the difference in the chemical composition of the passive films[63-65]. In nitric acid solution, the corrosion and passivation current density followed a pattern for bare 304 L SS > $Ni_{60}Nb_{30}Ta_{10}$> $Ni_{60}Nb_{30}Zr_{10}$ metallic glassy coating. The lower corrosion resistance of the glassy coating is attributed to the formation of the stable passive film on the surface. The surface morphology after potentiodynamic anodic polarization in nitric acid is depicted in Figure 11 (c-d). Bare 304 L SS is severely corroded along the grain boundary (Fig. 11a), while a relatively smooth and stable passive film is formed on the MGCs.

The XPS study was carried out to understand the high corrosion resistance behavior of MGCs after polarization in a nitric acid environment (Fig. 12).

After polarization test till 1.6 V (Ag/AgCl), all the metal oxides at their corresponding binding energies have been characterized on the surface of passivated MGCs and shown in Fig. 12(a-b). The passive film predominantly comprised Nb_2O_5 and Ta_2O_5 oxide at their corresponding binding energies on $Ni_{60}Nb_{30}Ta_{10}$ MGC; however, the passive film was enriched with Nb_2O_5 and ZrO_2 on the surface $Ni_{60}Nb_{30}Zr_{10}$ MGC. In both cases, Ni-oxide (NiO_2, Ni_2O_3) was also detected on the coating surface. The observed corrosion parameter differences mainly depends on the chemistry of the passive film, whereas the mixed Nb, Ta-pentaoxide provides slightly more corrosion resistance than Nb and Ta-pentaoxide. The schematic diagram representing the passive layer formation in 11.5 M nitric acid medium of (a) $Ni_{60}Nb_{30}Ta_{10}$ metallic glass coating, (b) $Ni_{60}Nb_{30}Zr_{10}$ metallic glass coating, is shown in Fig 13. The passive films are composed mostly of oxide of Nb_2O_5 and Ta_2O_5 for $Ni_{60}Nb_{30}Ta_{10}$ metallic glass

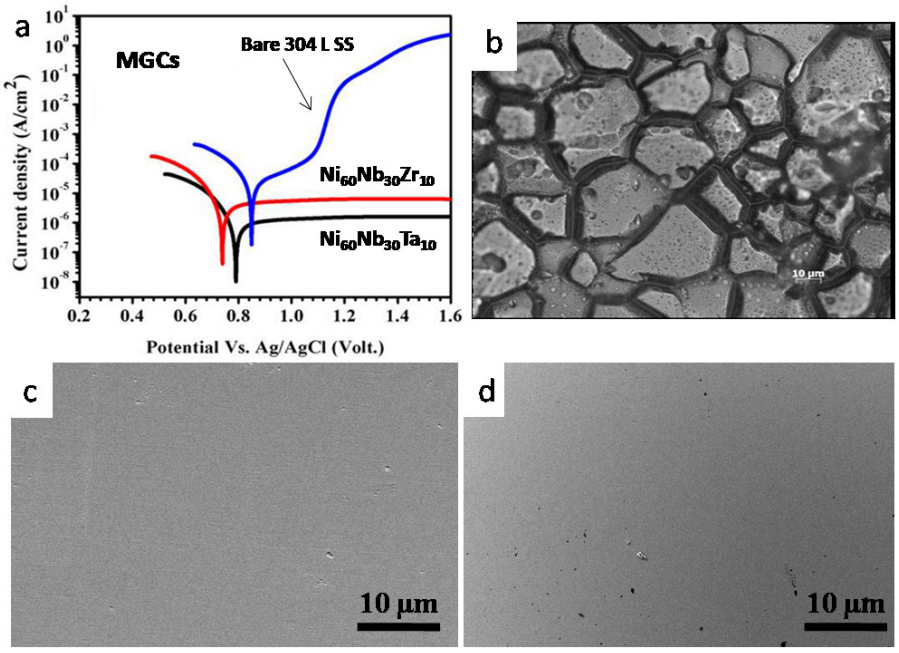


Figure 11. **(a)** The polarization test of $Ni_{60}Nb_{30}Ta_{10}$, $Ni_{60}Nb_{30}Zr_{10}$ metallic glass coatings and bare 304 L SS in 11.5 M nitric acid solution; Surface morphology (Optical images) after polarization test in 11.5 M nitric acid of **(a)** bare 304 L SS sample, **(b)** $Ni_{60}Nb_{30}Ta_{10}$. and **(b)** $Ni_{60}Nb_{30}Zr_{10}$ metallic glass coatings[9].

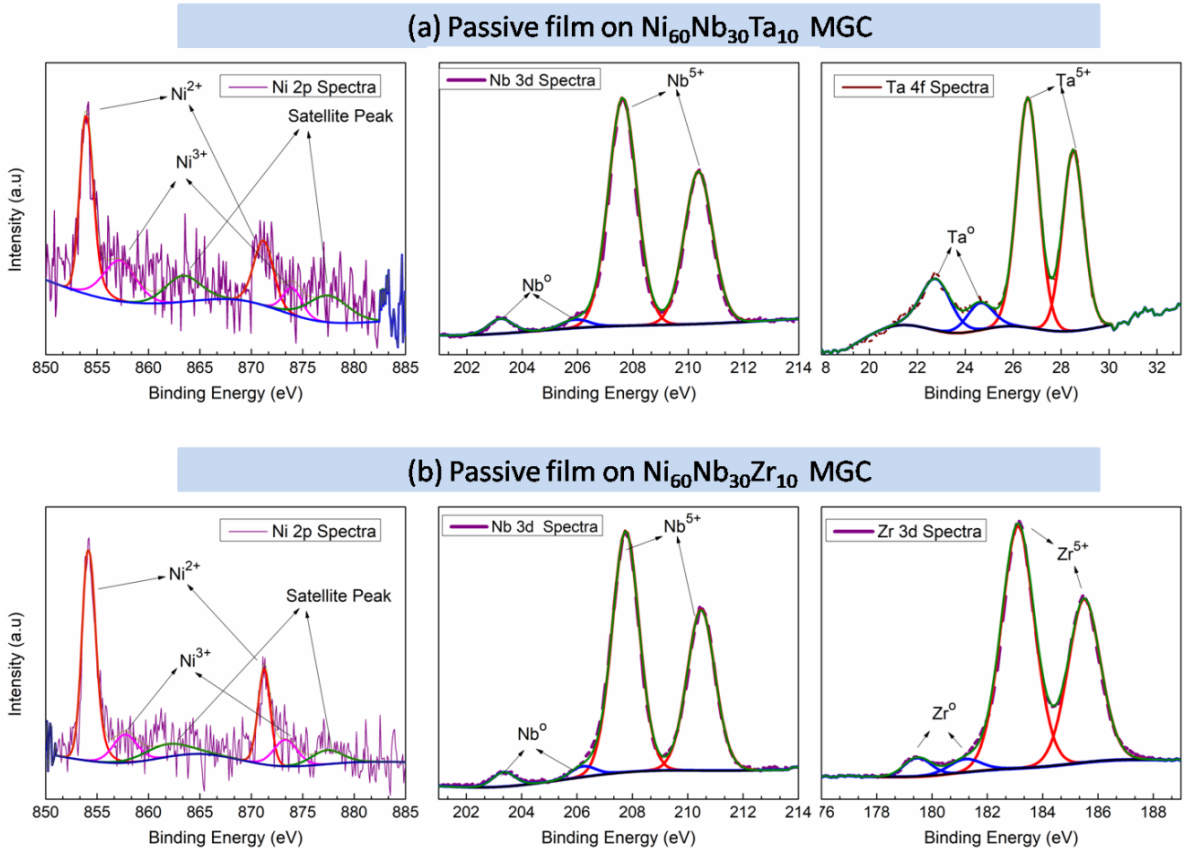


Figure 12. Passive film composition after polarization of **(a)** $Ni_{60}Nb_{30}Ta_{10}$, and **(b)** $Ni_{60}Nb_{30}Zr_{10}$ metallic glass coatings[9].

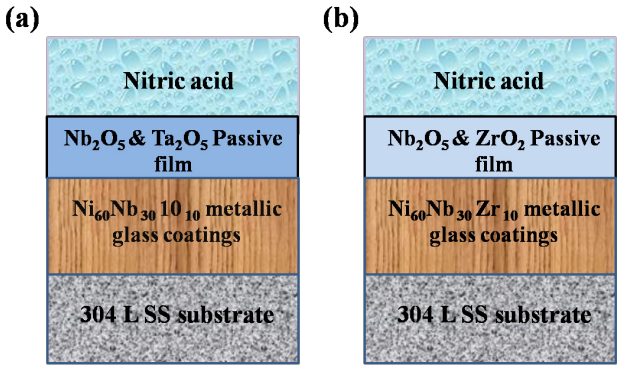


Figure 13. Schematic diagram representing the passive layer formating in 11.5 M nitric acid medium of **(a)** $Ni_{60}Nb_{30}Ta_{10}$ metallic glass coating, **(b)** $Ni_{60}Nb_{30}Zr_{10}$ metallic glass coating[9].

coating and Nb_2O_5 and ZrO_2 for $Ni_{60}Nb_{30}Zr_{10}$ metallic glass coating, which influences the corrosion resistance in nitric acid.

7. Challenges and Future Perspective

The metallic glasses coatings endow a wide range of opportunities for discovering and applying a class of coatings with exciting combinations of materials properties that are not achievable by cast bulk metallic glass alloys. Moreover, the MGCs open a wide window for corrosion engineers to be explored; however, many challenges are associated with developing MGCs as a corrosion resistant materials for industrial components. Even though the MGCs synthesized by magnetron sputtering are very dense, with smooth morphologies, and uniform microstructures with lower surface roughness, the main challenges are associated with applying a coating on large industrial components. Other techniques like cold and thermal spray were also applied for MGCs coating to the large substrate, but the coatings are associated with pores that can lead to a higher corrosion in aggressive environments. The pulsed laser technique increases the MGCs coating production costs, usually taking much time and a vast number of laser shots to achieve a higher coating thickness. By PLD techniques, only nano-meter level coating thickness can be achieved. Another challenge associated with developing MGCs with good GFA includes a noble metal, Pd, which may obstruct the wide-reaching purpose of MGCs in corrosion applications because of increased coatings production costs. However, adding toxic elements, like Be, might increase GFA for bio-medical corrosion applications, but it is a significant bio-safety concern.

Although the Zr and Ni-based MGCs exhibit excellent corrosion resistance in nitric acid at room temperature, except they undergo pitting corrosion in aggressive halide ions environments[25,62]. In addition, they are unstable under hot gas oxidation and hydrothermal conditions; thus, they cannot be applicable in such an environment for a longer time span[65]. The main reason is the coatings physical and chemical irregularities (large globules, pores, cracks, chemical agglomeration, etc.), which act as preferential pitting initiation sites and rapidly pits propagation into the highly reactive amorphous phase.[25] The defects formation can barely be avoided during MGCs preparation by magnetron sputtering. Pitting corrosion which can be initiated from such defects can be minimize/inhibit only by developing coating compositions with extremely high passivation ability elements. However, trans-passivity and pitting corrosion are also found on Ni-Nb MGCCs in chloride environments.[62] The addition of tantalum (Ta) and phosphorus can be beneficial in resisting pitting corrosion.[66]

The main future interest also involves studying the effect of different corrosive environments on coating-substrate interfacial corrosion failure, hydrogen stress cracking, hydrogen embrittlement, hydride formation, hydrogen blistering, and stress-corrosion cracking behavior of multifunctional MGCs samples. There are significant opportunities to improve the fundamental understanding of corrosion behavior under the mechanical stress of these emerging MGCs. Additional work in this regard might develop materials properties database and guidelines for designers and engineers for large scale industrial component.

8. Conclusions

MGCs can be an alternative to bulk metallic glasses. In the future, metallic glass coating can also potentially replace current electronic circuits (MEMS), solar cells, sensors, detectors, and corrosion-resistant coating. In the last decades, research has been intensifying on many MGCs of different compositions and their physical and chemical phenomena in disordered, non-equilibrium, multi-component films. Such outstanding properties provide great promise as one of the best and most desirable coatings for corrosion resistance applications. Apart from the fundamental studies, researchers also

need to focus on obtaining large-scale production of these coatings on the significant industrial component using cold and thermal spray techniques without creating large pores. The Zr and Ni-based metallic glass coatings or thin films can be produced with an amorphous structure by magnetron sputtering; thereby, the mass production of these MGCs is more beneficial as they are used for various applications. The present overview covers the microstructure and surface morphologies, and the corrosion properties of the various Zr and Ni-based metallic glass coatings and their degradation behavior in various corrosive media like NaCl, HCl, and HNO_3. It is worth noting that Zr and Ta in Ni-Nb metallic glass coating results in a stable passive film in a highly aggressive and concentrated nitric acid (11.5 M) environment. Also, Ni-based MGCs with remarkable properties in different environments can be explored for their application in different aggressive environments. The challenges and future perspective of BMG and their coatings present a promising area as components for engineering applications and materials science, offering many unique and interesting properties like higher strength, extremely low roughness, antibacterial characteristics, hardness, and corrosion resistance. However, challenges related to brittleness, surface finish, cost, ductility, manufacturing of thicker components, better glass forming ability, and processing difficulties hinder their widespread and commercial application. The BMGs and their coatings market are soon set for rapid expansion. Future research focuses on overcoming these limitations through strategies like developing compatible BMG matrix composites, improving processing techniques (especially additive manufacturing), and exploring new alloy compositions are require and essential. Further, use of magnetron sputtering for BMG coatings appears favourable for industries and manufacturers applications where technologies transfer from laboratory scale to factory is being explore.

9. References

1. Wang, CY, Hou JF, Dong ZC, and Zhang ZQ. The Zr-doped Mg-Zn-Ca bulk metallic glasses have high compressive strength, distinct plasticity, and good corrosion resistance. J. Non-Crystalline Solids. 2025; 652, 123397. https://doi.org/10.1016/j.jnoncrysol.2025.123397
2. Zhang SD, Wu J, Qi WB, and Wang JQ. Effect of porosity defects on the long-term corrosion behaviour of Fe-based amorphous alloy coated mild steel. Corros. Sci. 2016; 110, 57-70. https://doi.org/10.1016/j.corsci.2016.04.021
3. Kamachi Mudali U, Scudino S, Eckert J, and Gebert A. Corrosion behaviour of amorphous, quasicrystalline, nanostructured and crystalline Zr57Ti8Nb2.5Cu13.9Ni11.1Al7.5 alloy in acidic media. Scripta. Mater. 2004; 50, 1379-1384. https://doi.org/10.1016/j.scriptamat.2004.02.039
4. Kamachi Mudali U, Kühn U, Gebert A and Eckert J. Corrosion behaviour of zirconium based bulk metallic glasses. Transactions IIM. 2006; 59, 123-138.
5. Bahrami F, Amini R and Taghvaei AH. Microstructure and corrosion behavior of electrodeposited Ni-based nanocomposite coatings reinforced with Ni60Cr10Ta10P16B4 metallic glass particles. J. Alloys Compd. 2017; 714, 530-536. https://doi.org/10.1016/j.jallcom.2017.04.069
6. Jeong U, Han J, Marimuthu KP, Lee Y and Lee H. Evaluation of mechanical properties of Zr-Cu-Al-Ni TFMG using nanoindentation. J. Mater. Res. Technol. 2021; 12, 2368-2382. https://doi.org/10.1016/j.jmrt.2021.04.030
7. Cao QP, Liu JW,Yang KJ, Xu F, Yao ZQ, Minkow A, Fecht HJ, Ivanisenko J, Chen LY, Wang XD, Qu SX, and Jiang JZ. Effect of pre-existing shear bands on the tensile mechanical properties of a bulk metallic glass. Acta Mater. 2010; 58, 1276-1292. https://doi.org/10.1016/j.actamat.2009.10.032
8. Jayaraj J, Thinaharan C, Ningshen S, Mallika C and Kamachi Mudali U. Corrosion behavior and surface film characterization of TaNbHfZrTi high entropy alloy in aggressive nitric acid medium. Intermetallics. 2017; 89, 123-132 https://doi.org/10.1016/j.intermet.2017.06.002
9. Chiranjit Poddar. Electrochemical and corrosion behavior of Ni-based amorphous alloys and coatings for nitric acid application. PhD, Homi Bhabha National Institute, Mumbai, India. 2019.
10. Schroers J. Processing of bulk metallic glass. Adv. Mater. 2010; 22, 1566-1597. https://doi.org/10.1002/adma.200902776
11. Yiu P, Diyatmika W, Bönninghoff N, Lu YC, Lai BZ and Chu JP. Thin film metallic glasses: properties, applications and future. J. Appl. Phys. 2020; 127, 1-16. https://doi.org/10.1080/10942912.2019.1707221 https://doi.org/10.1080/10942912.2020.1792925
12. Axinte E. Metallic glasses from " Alchemy" to pure science: present and future of design, processing and applications of glassy metals. Mater. Des. 2012; 35, 518-556. https://doi.org/10.1016/j.matdes.2011.09.028
13. Schroers J, Bulk metallic glasses. Phys. Today. 2013; 66, 32-37. https://doi.org/10.1063/PT.3.1885
14. Johnson WL. Bulk glass-forming metallic alloys: science and technology. MRS Bull. 1999; 24, 42-56. https://doi.org/10.1557/S0883769400053252

15. Hu HT, Chen LY, Wang XD, Cao QP, and Jiang JZ. Formation of Ni - Nb - Zr - X (X = Ti, Ta, Fe, Cu, Co) bulk metallic glasses. J. Alloys Compd. 2008; 460, 714-718. https://doi.org/10.1016/j.jallcom.2008.01.075
16. Scully JR, Gebert A, and Payer JH. Corrosion and related mechanical properties of bulk metallic glasses. J. Mater. Res. 2007; 22, 302-313. https://doi.org/10.1557/jmr.2007.0051
17. Pang SJ, Zhang T, Asami K, and Inoue A. New Fe-Cr-Mo-(Nb, Ta)-C-B glassy alloys with high glass forming ability and good corrosion resistance. Mater. Trans. JIM. 2001; 42, 376-379. https://doi.org/10.2320/matertrans.42.376
18. Poddar C, Jayaraj J, Mallika C, and Kamachi Mudali U. Oxidation behaviour of Ni60Nb30Ta10 metallic glass below its glass transition temperature. J. Alloys Compd. 2017; 728, 1146-1152. https://doi.org/10.1016/j.jallcom.2017.09.040
19. Jayaraj J, Kim KB, Ahn HS, and Fleury E. Corrosion mechanism of N-containing Fe-Cr-Mo-Y-C-B bulk amorphous alloys in highly concentrated HCl solution, Mater. Sci. Eng. 2007; 448-451, 517-520. https://doi.org/10.1016/j.msea.2006.02.418
20. Han MK, Kim JY, Hwang MJ, Song HJ, and Park YJ. Effect of Nb on the microstructure, mechanical properties, corrosion behavior, and cytotoxicity of Ti-Nb alloys. Materials. 2015; 8, 5986-6003. https://doi.org/10.3390/ma8095287
21. Zander D, Heisterkamp B, and Gallino I. Corrosion resistance of Cu-Zr-Al-Y and Zr-Cu-Ni-Al-Nb bulk metallic glasses. J. Alloys Compd. 2007; 434-435, 234-236. https://doi.org/10.1016/j.jallcom.2006.08.112
22. Schroeder V, Gilbert CJ and Ritchie RO. Comparison of the corrosion behavior of a bulk amorphous metal, Zr41.2Ti13.8Cu12.5Ni10Be22.5, with its crystallized form. Scr. Mater.1998; 38, 1481-1485. https://doi.org/10.1016/S1359-6462(98)00089-X
23. Wang DP, Wang SL and Wang JQ. Relationship between amorphous structure and corrosion behaviour in a Zr-Ni metallic glass. Corros. Sci. 2012; 59, 88-95. https://doi.org/10.1016/j.corsci.2012.02.017
24. Green BA, Meyer HM, Benson RS, Yokoyama Y, Liaw PK, and Liu CT. A study of the corrosion behaviour of Zr50Cu(40-X) Al10PdX bulk metallic glasses with scanning auger microanalysis. Corros. Sci. 2008; 50, 1825-1832. https://doi.org/10.1016/j.corsci.2008.03.011
25. Ningshen S, Kamachi Mudali U, Krishnan R, and Raj B. Corrosion behavior of Zr-based metallic glass coating on type 304L stainless steel by pulsed laser deposition method. Surf. Coatings Technol. 2011; 205, 3961-3966. https://doi.org/10.1016/j.surfcoat.2011.02.039
26. Poddar C, Jayaraj J, and Ningshen S. Passive film characteristics and corrosion behavior of thermally oxidized Ni60Nb30Ta10 metallic glass in nitric acid medium. J. Alloys Compd. 2019; 783, 680-686. https://doi.org/10.1016/j.jallcom.2018.12.335
27. Poddar C, Jayaraj J, Ningshen S, Kamachi U, and Mudali UK. Effect of thermal oxidation on the oxide characteristic and corrosion behavior of Ni 60 Nb 40 amorphous ribbon in nitric acid. Appl. Surf. Sci. 2019; 479, 430-439. https://doi.org/10.1016/j.apsusc.2019.02.089
28. Poddar C, Jayaraj J, Amirthapandian S, and Ningshen S. Effect of thermally grown amorphous oxide film on the corrosion resistance properties of Ni50Zr25Nb25 metallic glass in nitric acid medium. Intermetallics. 2019; 113, 106571. https://doi.org/10.1016/j.intermet.2019.106571
29. Greer AL, Cheng YQ, and Ma E. Shear bands in metallic glasses. Mater. Sci. Eng. R. 2013; 74, 71-132. https://doi.org/10.1016/j.mser.2013.04.001
30. Rajan ST, Nanda Kumar AK, and Subramanian B. Nanocrystallization in magnetron-sputtered Zr-Cu-Al-Ag thin film metallic glasses. Cryst. Eng. Comm. 2014; 16, 2835-2844. https://doi.org/10.1039/C3CE42294A
31. Rajan ST and Arockiaraja A. A Thin film metallic glasses for bioimplants and surgical tools: a review. J. Alloys Compd. Elsevier. 2021; 876, 159939. https://doi.org/10.1016/j.jallcom.2021.159939
32. Rauf A, Guo CY, Fang YN, Yu Z, Sun BA and Feng T. Binary Cu-Zr thin film metallic glasses with tunable nanoscale structures and properties. J. Non. Cryst. Solids. 2018; 498, 95-102. https://doi.org/10.1016/j.jnoncrysol.2018.06.015
33. Chu JP, Huang JC, Jang JSC, Wang YC and Liaw PK. Thin film metallic glasses: preparations, properties, and applications. JOM. 2010; 19-24. https://doi.org/10.1007/s11837-010-0053-3
34. Huang JC, Chu JP and Jang JSC. Recent progress in metallic glasses in Taiwan, Intermetallics. 2009; 17, 973-987. https://doi.org/10.1016/j.intermet.2009.05.004
35. Ham GS, Kim KW, Cho GS, Kim CP and Lee KA. Fabrication, microstructure, and wear properties of novel Fe-Mo-Cr-C-B metallic glass coating layers manufactured by various thermal spray processes. Mater. Des. 2020; 195:109043. https://doi.org/10.1016/j.matdes.2020.109043
36. Chu CW, Jang JSC, Chiu SM, and Chu JP. Study of the characteristics and corrosion behavior for the Zr-based metallic glass thin film fabricated by pulse magnetron sputtering process. Thin Solid Films. 2009; 517, 4930-4933. https://doi.org/10.1016/j.tsf.2009.03.049
37. Ni HS, Liu XH, Chang XC, Hou WL, Liu W, and Wang JQ. High-performance amorphous steel coating prepared by HVOF thermal spraying. J. Alloys Compd. 2009; 467, 163-167. https://doi.org/10.1016/j.jallcom.2007.11.133
38. Lee J, Huang KH, Hsu KC, Tung HC, Lee JW, and Duh JG. Applying composition control to improve the mechanical and thermal properties of Zr-Cu-Ni-Al thin film metallic glass by magnetron DC sputtering. Surf. Coatings Technol. 2015; 278,132-137. https://doi.org/10.1016/j.surfcoat.2015.07.015

39. Chen PS, Chen HW, Duh JG, Lee JW, and Jang JSC. Characterization of mechanical properties and adhesion of Ta-Zr-Cu-Al-Ag thin film metallic glasses. Surf. Coatings Technol. 2013; 231, 332-336. https://doi.org/10.1016/j.surfcoat.2012.03.087
40. Subramanian B, Maruthamuthu S, and Rajan ST. Biocompatibility evaluation of sputtered zirconium-based thin film metallic glass-coated steels. Int. J. Nanomedicine. 2015; 10, 17-29. https://doi.org/10.2147/IJN.S79977
41. Korkmaz S and Kariper A. Glass formation, production and superior properties of Zr-based thin film metallic glasses (TFMGs): a status review. J. Non. Cryst. Solids. 2020; 527, 119753. https://doi.org/10.1016/j.jnoncrysol.2019.119753
42. Apreutesei M, Boissy C, Mary N, Arab Pour Yazdi M, Billard A, and Steyer P. Binary Zr-Ni/Co metallic glass films: role of the structural state on their durability. Acta Mater. 2015; 89, 305-314. https://doi.org/10.1016/j.actamat.2015.01.056
43. Apreutesei M, Djemia P, Belliard L, Abadias G, Esnouf C, Billard A, and Steyer P. Structural-elastic relationships of Zr-TL (TL = Cu, Co, Ni) thin films metallic glasses. J. Alloys Compd. 2017; 707, 126-131. https://doi.org/10.1016/j.jallcom.2016.12.208
44. A. Inoue A, Wang XM, and Zhang W. Developments and applications of bulk metallic glasses. Rev. Adv. Mats. Sci. 2008; 18, 1-9. https://doi.org/10.1007/978-0-387-48921-6_1
45. Deng YL, Lee JW, Lou BS, Duh JG, Chu JP, and Jang JSC. The fabrication and property evaluation of Zr-Ti-B-Si thin film metallic glass materials. Surf. Coatings Technol. 2014; 259, 115-122. https://doi.org/10.1016/j.surfcoat.2014.03.026
46. Jiang L, Chen ZQ, Lu HB, Ke HB, Yuan Y, Dong YM, and Meng XK. Corrosion protection of NiNb metallic glass coatings for 316SS by magnetron sputtering. J. Mater. Sci. Technol. 2021; 79, 88-98. https://doi.org/10.1016/j.jmst.2020.12.004
47. Zeman P, Zítek M, Zuzjaková, and Čerstvý R. Amorphous Zr-Cu thin-film alloys with metallic glass behavior. J. Alloys Compd. 2017; 696, 1298-1306. https://doi.org/10.1016/j.jallcom.2016.12.098
48. Chen CJ, Huang JC, Chou HS, Lai YH, Chang LW, Du XH, Chu JP, and Nieh TG. On the amorphous and nanocrystalline Zr-Cu and Zr-Ti co-sputtered thin films. J. Alloys Compd. 2009; 483, 337-340. https://doi.org/10.1016/j.jallcom.2008.07.188
49. Ran He R, Fei Li M, Malomo B, and Yang L. Enhancing corrosion and mechanical properties of 304 stainless steel by depositing and annealing Zr75Cu25 thin-film metallic glass. Surf. Coatings Technol. 2020; 400, 126221. https://doi.org/10.1016/j.surfcoat.2020.126221
50. Diyatmika W, Yu CC, Tanatsugu Y, Yasuzawa M, and Chu JP. Fibrinogen and albumin adsorption profiles on Ni-Free Zr-based thin film metallic glass. Thin Solid Films. 2019; 688, 137382. https://doi.org/10.1016/j.tsf.2019.06.032
51. Chuang CY, Liao YC, Lee JW, Li CL, Chu JP, and Duh JG. Electrochemical characterization of Zr-based thin film metallic glass in hydrochloric aqueous solution. Thin Solid Films. 2013; 529, 338-341. https://doi.org/10.1016/j.tsf.2012.03.065
52. Lee J and Duh JG. Structural evolution of Zr-Cu-Ni-Al-N thin film metallic glass and its diffusion barrier performance in Cu-Si interconnect at elevated temperature, vacuum.2017; 142, 81-86. https://doi.org/10.1016/j.vacuum.2017.05.009
53. Chuang CY, Lee JW, Li CL, and Chu JP. Mechanical properties study of a magnetron-sputtered Zr-based thin film metallic glass. Surf. Coatings Technol. 2013; 215, 312-321. https://doi.org/10.1016/j.surfcoat.2012.04.101
54. Park KW, Il Jang J , Wakeda M, Shibutani Y, and Lee JC.Atomic packing density and tts influence on the properties of Cu-Zr amorphous alloys. Scr. Mater. 2007; 57, 805-808. https://doi.org/10.1016/j.scriptamat.2007.07.019
55. Chuang MH, Wang C, Chao BK, Kao WL, Shyue JJ, and Hsueh CH. Mechanical properties and microstructure of Zr-Ti-Ni thin film metallic glasses modified with minor SF6. Compos. Part B Eng. 2017; 129, 243-250. https://doi.org/10.1016/j.compositesb.2017.07.032
56. Alvarez R, Garcia-Martin JM, Garcia-Valenzuela A, Macias-Montero M, Ferrer FJ, Santiso J, Rico V, Cotrino J, Gonzalez-Elipe AR, and Palmero A. Nanostructured Ti thin films by magnetron sputtering at oblique angles. J. Phys. D. Appl. Phys. 2015; 49, 045303. https://doi.org/10.1088/0022-3727/49/4/045303
57. Ketov SV, Joksimovic R, Xie G, Trifonov A, Kurihara K and Louzguine-Luzgin DV. Formation of nanostructured metallic glass thin films upon sputtering. Heliyon. 2017; 3, e00228. https://doi.org/10.1016/j.heliyon.2016.e00228
58. Zhang BP, Kawashima A, Habazaki H, Asami K, and Hashimoto K. The effect of structural heterogeneity on the pitting corrosion behavior of melt-spun amorphous Ni-Zr alloys. Corros. Sci. 1997; 39, 2005-2018. https://doi.org/10.1016/S0010-938X(97)00091-7
59. Nak M, Hashimoto K, and Masumoto T. Corrosion behavior of amorphous and crystalline Cu50Ti50 and Cu50Zr50 alloys. J. Non. Cryst. Solids. 1978; 30, 29-36. https://doi.org/10.1016/0022-3093(78)90053-4
60. Tang J, Zhu Q, Wang Y, Apreutesei M, Wang H, Steyer P, Chamas M, and Billard A. Insights on the role of copper addition in the corrosion and mechanical properties of binary Zr-Cu metallic glass coatings. Coatings. 2017; 7, 223. https://doi.org/10.3390/coatings7120223
61. Kamachi Mudali U, Baunack S, Eckert J, Schultz L, and Gebert A. Pitting corrosion of bulk glass-forming

zirconium-based alloys. J. Alloys Compd. 2004; 377, 290-297. https://doi.org/10.1016/j.jallcom.2004.01.043

62. Wu ZF, Cao QP, Ma Y, Wang C, Liu SY, Qian X, Wang XD, and Jiang JZ. Thickness-dependent pitting corrosion behavior in Ni-Nb thin film metallic glass. Thin Solid Films. 2014; 564, 294-298 https://doi.org/10.1016/j.tsf.2014.06.019
63. Poddar C, Ningshen S and Jayaraj J. Corrosion assessment of Ni60 Nb30Ta10 metallic glass and ts partially crystallized alloy in concentrated nitric acid environment. J. Alloys Compd. 2020; 813, 152172. https://doi.org/10.1016/j.jallcom.2019.152172
64. Jang JSC, Tsai PH, Shiao AZ, Li TH, Chen CY, Chu JP, Duh JG, Chen MJ, Chang SH and Huang WC. Enhanced cutting durability of surgical blade by coating with Fe-based metallic glass thin film. Intermetallics. 2015; 65, 56-60. https://doi.org/10.1016/j.intermet.2015.06.012
65. Jiang L, Chen ZQ, Lu HB, Ke HB, Yuan Y, Dong YM and Meng XK. Corrosion protection of NiNb metallic glass coatings for 316SS by magnetron sputtering. J. Mater. Sci. Technol. 2021; 79, 88-98. https://doi.org/10.1016/j.jmst.2020.12.004
66. Wang W, Mraied H, Diyatmika W, Chu JP, Li L and Cai W. Effects of nanoscale chemical heterogeneity on the wear, corrosion, and tribocorrosion resistance of Zr-based thin film metallic glasses. Surf. Coatings. Tech. 2020; 402, 126324. https://doi.org/10.1016/j.surfcoat.2020.126324